Bioorganic Chemistry 93 (2019) 103332

Contents lists available at ScienceDirect

Bioorganic Chemistry

journal homepage: www.elsevier.com/locate/bioorg

Towards breast cancer targeting: Synthesis of tetrahydroindolocarbazoles, antibreast cancer evaluation, uPA inhibition, molecular genetic and molecular modelling studies

Entesar M. Ahmed[a,*], Alaadin E. Sarhan[b], Dina H. El-Naggar[c], Reham R. Khattab[d], Mohamed El-Naggar[e], Shahenda M. El-Messery[f,*], Ghada S. Hassan[g], Marwa M. Mounier[h], Khaled Mahmoud[h], Neama I. Ali[i], Karima F. Mahrous[i], Mamdouh M. Ali[j], Mardia T. El Sayed[c,*]

[a] Chemistry Department, Faculty of Science, Al-Azhar University (Girls Branch), Cairo, Egypt
[b] Therapeutical Chemistry Department, Pharmaceutical Division, National Research Centre, Dokki- 12311, Egypt
[c] Department of Applied Organic Chemistry, National Research Centre, 12622 Dokki, Giza, Egypt
[d] Photochemistry Department, Chemical Industries Research Division, National Research Centre, Dokki 12311, Egypt
[e] Chemistry Department, Faculty of Sciences, University of Sharjah, Sharjah 27272, United Arab Emirates
[f] Department of Pharmaceutical Organic Chemistry, Faculty of Pharmacy, Mansoura University, 35516 Mansoura, Egypt
[g] Department of Medicinal Chemistry, Faculty of Pharmacy, Mansoura University, 35516 Mansoura, Egypt
[h] Pharmacognosy Department, National Research Centre, 12622-Dokki, Egypt
[i] Cell Biology Department, National Research Centre, 12622-Dokki, Egypt
[j] Biochemistry Department, National Research Centre, 12622-Dokki, Egypt

ARTICLE INFO

Keywords:
Breast cancer
Tetrahydroindolocarbazoles
Urokinase inhibition
DNA genetics
Molecular modelling studies

ABSTRACT

A series of some new tetrahydroindolocarbazole derivatives has been synthesized. The structure of the synthesized compounds has been confirmed by different spectroscopic techniques such as IR, NMR, elemental analysis and mass spectrometry. The target compounds were evaluated for their antitumor activity against breast cancer cell line MCF-7, their GI% and their LC_{50} have been determined. Six of the synthesized compounds exhibited GI% values against MCF-7 cell lines exceeding **70**% ranging from **71.9 to 85.0**% in addition that compound **11** expressed GI% values of **99.9%** and considered the most active derivatives among the synthesized ones. Compound **11** showed a remarkable decrease of u PA level to **3.5** ng/ml compared to DOX. Compound **5, 11** and **15** showed significant decrease in expression of MTAP and CDKN2A, in addition to a remarkable decrease in DNA damage comet assay method. Molecular modeling studies were performed to interpretate the behavior of active ligands as uPA inhibitors.

1. Introduction

Urokinase is a type of protease enzyme also known as urokinase plasminogen activator (uPA), it is a serine type of protease enzyme that is present in humans and animals. It is mainly present in the blood and extracellular matrix (ECM) of the tissues and involved in either vascular diseases or cancer progression [1,2]. Increased level of urokinase expression with other plasminogen activation system was found to be in correlation with tumour malignancy *via* tissue degradation- facilitates tissue invasion and promotes metastasis as it is implicated in different physiological and pathological processes including cell migration, angiogenesis, inflammation, tumour growth and metastasis. It was also found that uPA was overexpressed in different types of human malignant tumour such as colon, liver, breast, lung, stomach and ovarian cancer, when compared to normal cells also uPA has been used a tumor "marker". Accordingly, urokinase inhibitors have been sought to be used as anticancer agents [3,4]. Breast cancer is considered the second cause of cancer-related deaths in women all over the world. Multiple drugs have been approved by the US-FDA for treatment of breast related malignancies. Frequent emergence of resistances leads to the urgent need for newer moieties to overcome such problems [5]. Recently, amiloride HCl -which has been used for decades as potassium sparing diuretic- also proved to exhibit significant antitumor and antimetastasis activities in biochemical, cellular and animal tumor models. Several studies have established that amiloride can suppress the metastases formation and the invasive capacity of human breast cancer

* Corresponding authors.
E-mail addresses: entsar.ahmed2016@yahoo.com (E.M. Ahmed), selmessery@gmail.com (S.M. El-Messery), mardia.elsayed2016@gmail.com (M.T. El Sayed).

https://doi.org/10.1016/j.bioorg.2019.103332
Received 7 March 2019; Received in revised form 7 August 2019; Accepted 28 September 2019
Available online 01 October 2019

cell lines of types MDA-MB-231 and MDA-MB-436 in a dose dependant manner. Through studying its mechanisms of action, it was revealed that one of the methods to inhibit the breast cancer propagation is through the inhibition of uPA system by binding reversibly to the enzyme's active site, [6]. Furthermore, many researchers correlate between the level of expression of uPA and the progression of breast cancer. Previously, the traditional prognosis of breast cancer focused on age, tumour size, tumour grade and lymph node status etc [7,8], but as uPA was found to be involved in regulating breast cancer invasion due to its ability to facilitate (ECM) degradation, cell proliferation, migration and adhesion, it becomes the first novel tumour prognostic factors confirmed un highest level of evidence regarding the clinical utility in breast cancer [9]. Drugs targeting breast cancer with various indole based derivatives have also been explored [10a,b,11a,b]. Indole products using DNA- established electrochemical biosensors evidenced that it can meaningfully lessen the advancement of cancer cell lines such as HOP-92 (lung), A498 (renal) and MDAMB-231/1TCC (breast) [12,13a]. Indoles and Indolocarbazoles have also promising anti-breast cancer potential [13b], in addition, that was related to DNA expression [14,15]. That possible role of indole based anticancer agents typically for the breast related malignancies Fig. 1A and B has put an emphasis on the synthesis of new derivatives to overcome problems faced by existing therapeutic agents (see Scheme 1).

Taking into consideration the above-mentioned facts, and as a part of our ongoing effort to develop potent indole based anti-breast cancer agents [13b], in the present work a group of some new tetrahydroindolocarbazoles (THICZs) with variety of substituents has been synthesized and subjected to spectroscopic elucidation using different techniques such as IR, ^{1}HNMR, ^{13}CNMR, elemental analysis and mass spectroscopy. They were examined for their *in-vitro* antibreast cancer screening, progressive urokinase inhibition, DNA-damage determination were further evaluated. Computer modelling studies exhausting the energetic site of uPA as a template for the most active uPA inhibitors were calculated.

2. Results and discussion

2.1. Chemistry

The target compounds THICZs (**1–20**) were prepared by the use of two dissimilar synthetic methodologies according to the reported procedures [11,12]. The first method involved the preparation of the intermediates bis-indolylmethane (**BIMs**) by condensation of indole and different substituted aromatic aldehydes followed by reaction of equimolar concentration of both BIMs and the same aldehyde used in its preparation. The reaction proceeded in methanolic solution in presence of catalytic amount of concentrated H_2SO_4 added gently to the reaction mixture. An alternative method was used to synthesize the target compounds through one step reaction by the use of double amounts of both indole and the substituted aromatic aldehydes in methanol and in presence of catalytic amount of concentrated H_2SO_4. The compounds produced by both methods were identical according to the spectral data performed. It was also found that the direct method gave better yield ranging from 65 to 90%. All compounds (**1–20**) derived from aldehydes (**1–20**) were confirmed by means of analytical and spectral data. Compounds **1–8** and **18–20** were previously reported and their identities are equivalent to our reported samples [12,16]. These known derivatives have been synthesized to completely address the effect of structure modification whereas the THICZs (**9–17**) are new derivatives synthesized and confirmed by the means of ^{1}H- and ^{13}C NMR, ESI-MS and IR spectra. The ^{1}H NMR spectra of all these compounds showed singlet signal around δ from 4.5 to 5.5 ppm belonging for 2 protons of (2CH), the two NH indole protons appeared around δ from 9.94 to 10.4 ppm as a broad signal. The ^{1}H NMR data proved the similarity of the structure which confirmed additionally by its ^{13}C NMR spectrum (see Table 1).

2.2. Anticancer evaluation

The antitumor activity of the synthesized compounds has been performed against MCF-7 breast cancer cell line obtained from Vacsera (Giza, Egypt). Culturing and subculturing were carried out according to reported procedure; a negative control composed of DMSO was also used [17]. Cell % viability was evaluated and described according to the reported protocols [18,19]. The absorbance was measured consuming a microplate multi-well reader at 595 nm and a reference wavelength of 690 nm. Cell viability was evaluated rendering to the mitochondrial-supported reduction of yellow MTT (3-(4, 5-dimethylthiazol-2-yl)-2, 5- diphenyl tetrazolium bromide) to exaggerated formazan. The GI% (Growth inhibition percentage) of the synthesized compounds was illustrated in Table 2. It was observed that **6** of the synthesized compounds exhibited GI% values against MCF-7 cell lines exceeding **70**% ranging from **71.9 to 85.0**% in addition that compound **11** expressed GI% values of 99.9% and considered the most active derivatives among the synthesized ones. LC_{50} of the most active compounds were evaluated and illustrated in Table 2. In the same manner, compounds **11** and **15** exhibited the least LC_{50} values of **5.7** and **10.8** respectively.

2.3. Urokinase inhibition assay

One of the landscapes of a number of distortions counting lung, prostate, breast, and stomach cancers is the over-expression of the plasminogen activator urokinase (uPA) [20–22]. In the present work,

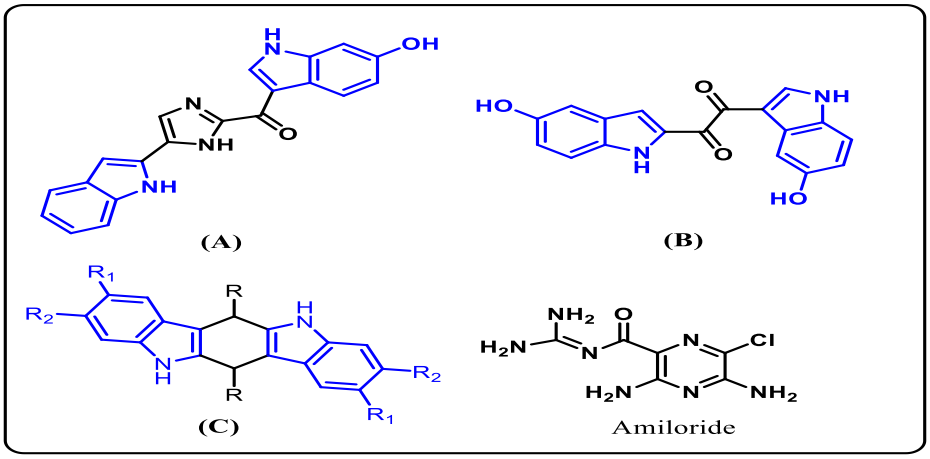

Fig. 1. Reported structures of anticancer indoles (A and B) and structures of synthesised derivatives (C).

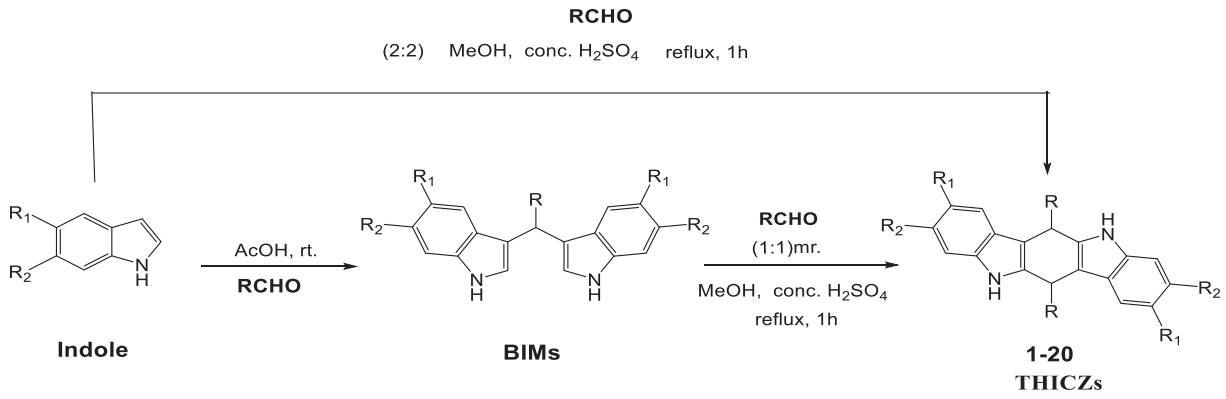

Scheme 1. Synthesis of THICZs.

Table 1
Structures of the synthesized THICZs.

Compound NO.	R1	R2	R
1	H	H	H
2	H	H	Ph
3	H	H	*p*-Br-Ph
4	H	H	*m*-Br-Ph
5	**H**	**H**	***p*-N(Me)$_2$-Ph**
6	H	H	*m*-OCH$_2$Ph-Ph
7	H	H	*p,m*-OH-Ph
8	H	H	*p*-MeO-*m*-OCH$_2$Ph-Ph
9	H	H	*m*-MeO-*p*-OCH$_2$Ph-Ph
10	H	H	*p*-OCH$_3$-Ph
11	**H**	**H**	***p*-CN-Ph**
12	H	H	2,4-di-NO$_2$-Ph
13	H	H	2,6-di-NO$_2$-Ph
14	H	H	*m*-OCH$_3$-Ph
15	**H**	**H**	***P*-OH,*m*-OCH$_3$-Ph**
16	H	H	2,5-OH-Ph
17	H	H	*p*-OCH$_2$Ph-Ph
18	H	Cl	*p*-MeO-*m*-OCH$_2$Ph-Ph
19	Cl	H	*p*-MeO-*m*-OCH$_2$Ph-Ph
20	H	H	*m*-Cl-Ph

Table 2
The GI% values of the target compounds, LC_{50} of the most active compounds.

Comp. No	GI%	LC_{50}	Comp. No	GI%	LC_{50}
2	29.5		**13**	**73.7**	**58.5 ± 1.3**
3	**77.7**	**63.5 ± 0.9**	14	8.30	
4	5.70		**15**	**85.00**	**10.8 ± 0.8**
5	**71.9**	**33.1 ± 0.6**	16	13.00	
6	**79.8**	**45.6 ± 1.1**	17	22.70	
8	33.00		18	13.30	
9	53.10		19	36.10	
10	22.60		20	29.90	
11	**99.9**	**5.7 ± 0.8**	Doxorubicin	100.00.	30.5 ± 2.1

Table 3
The level of expression of uPA protein in the MCF7 cells.

Compound	uPA level (ng/ml)
11	3.50 ± 0.47 [a]
15	11.00 ± 1.30 [a]
DMSO	22.00 ± 3.70
Dox	2.30 ± 0.37 [a]

Data are expressed as mean ± S.E. of three separate experiments.
[a] Is significant difference from control untreated at $p < 0.05$.

the decrease in the level of (uPA) expression was used to indicate the activity of the synthesized compounds as antitumor agents. The most active compounds **11** and **15** were used and tested for their ability to reduce the uPA protein expression. The levels of expression of uPA protein articulated in cell extracts of MCF7 cell line were illustrated in Table 3. The data revealed that, the concentrations of uPA protein were reduced when the cells were treated with compounds **11** and **15**, as compared with the untreated cancer cells (control) whose value was 22.00 ± 3.70 ng/ml, the levels of uPA protein in compounds **11** and **15** were decreased by 84% and 50% correspondingly with IC_{50} identical 3.50 ± 0.47 ng/ml for candidate **11** and for compound **15** it was 11.00 ± 1.30 ng/ml when compared with regulator cancer cells. Thus the decrement in the level of uPA protein manifestation are reliable with the cytotoxicity outcomes resulting in that the anticancer effect of tested composites may employ its anticancer activity by hindering uPA and possess significant anticancer activity comparable to the activity of the commonly used anticancer drug, doxorubicin [23–25].

2.4. Molecular genetics

2.4.1. Gene expression analysis

2.4.1.1. Quantitative real time PCR method. The sequences of specific primer of the genes used are listed in Table 4. The relative quantification of the target to the reference was determined by using the $2^{-\Delta\Delta CT}$ method as follows:

$$\Delta C_{T(test)} = C_{T(target,\ test)} - C_{T(reference,\ test)},$$
$$\Delta CT(calibrator) = C_{T(target,\ calibrator)} - C_{T(reference,\ calibrator)},$$
$$\Delta\Delta CT = \Delta C_{T(Test)} - \Delta C_{T(calibrator)}.$$

As illustrated in Figs. 2 and 3, in comparison to the positive control group, the transcription levels of MTAP and CDKN2A showed a non-significant reduction in both **11** and **15** cell lines and a significant decrease in cell line with compound **5**. Additionally, the expression levels of MTAP and CDKN2A genes for cell line with compound **5** exhibit a statistically significant decrease as compared to cell line **11** and a slight non-significant reduction as compared to cell line **15**.

2.4.1.2. DNA damage using comet assay. The neutral comet assay for tumor cell lines was used as described according to the reported procedures for compounds **5, 11** and **15**. For each sample about 100 cells were examined to determine the percentage of cells with DNA damage that appear like comets based on perceived comet tail length migration and relative proportion of DNA in the nucleus [26,27]. Behavior of **5**, **11** and **15** cell lines has discovered that DNA damage was amplified meaningfully as associated to the negative control group accomplishment 19.75, 17 and 16.25 in **11**, **15** and **5** compounds, correspondingly, while, the percentage of the scratched cells in these three compounds (**11**, **15** and **5**) was markedly decreased with a

Table 4
Primers sequence used for *RT-qPCR*.

Gene	Forward	Reverse
β-actin	GAT GCA GAA GGA GAT CAC TGC	AGT ACT TGC GCT CAG GAG GA
MTAP	CCA CCG CCG TGA AGA TTG GAA	CCA CCG CCG TGA AGA TTG GAA
CDKN2A	CCA CCG CCG TGA AGA TTG GAA	AAG TTT CCC GAG GTT TCT CA

MTAP : Methylthioadenosine Phosphorylase; CDKN2A: Cyclin Dependent Kinase Inhibitor 2A.

significant value for samples **15** and **5** and with a non-significant value for sample **11** tumor cell line as compared to the positive control group. Hence, the increase of un-fragmented cells values revealed a positive effect of compounds in comparing with the positive control group and the decrease of such values indicated that compounds have no effect on the studied cell lines as compared to the negative control group (Table 5).

2.5. Molecular modeling study

2.5.1. Docking studies

Conformational analysis of the most active uPA inhibitors have been performed in addition to Amiloride that was selcted as reference uPA inhibitor in our modeling study. The least energy conformer for each compound was obtained by conformational searching in torsional space using the multiconformer method and is illustrated in Fig. 4a–c. It was quite interesting to perform a docking study of the best uPA inhibitory activity synthesized compounds **11** and **15** respectively against **Amiloride** which was recognized recently as a lead compound for uPA inhibitors as anticancer agents [28–30].

The results obtained were quite informative. The complex structure of uPA and amiloride was used as a reference for modeling and docking (Fig. 5). It showed a tight binding occupying the S1 and S1β sites via excessive hydrogen bonding formation in addition to salt-bridge interaction with Asp189, in addition to important aminoacid in the binding pocket illustrated in Ser190, Gly219, Val227, Arg 217 and Lys 224, Ser 214 and Tryp 215, the binding energy was estimated by −12.987635 Kcal/mol [6].

Docking results revealed that compound **11** has shown high affinity with a binding energy of −11.3456 Kcal/mol with Ser192 and Gly A216 *via* hydrogen bonding type of interaction (64%) and (92%) respectively while Arg217 amino acid residue binds with both aryl part of indole ring by arene-arene interaction type (Fig. 6). Moreover, Compound **15** binds well with good affinity binding energy of −12.8776 Kcal/mol with Arg 217 and Leu 222 by an arene-arene interaction while it binds with Gly 216 by a hydrogen binding interaction through its (31%) (Fig. 7).

A deep insight to the interaction of synthesized uPA inhibitors **11** and **15** showed their interact action with the importants amino acid residue in the active site of uPA enzyme such as the cocrystallized ligand explaining their activity profile inspite of their dissimilarity in structure to the reference amiloride under study. A detailed view of both compounds **15** into the active site, have shown that it occupies a

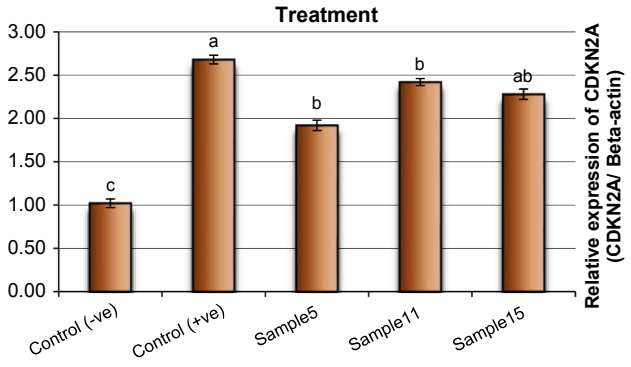

Fig. 3. The alterations of CDKN2A gene in tumor cell lines treated. Data are presented as mean ± SEM. [a–c]Mean values within tissue with unlike superscript letters were significantly different ([a:] $P < 0.01$, [b and c] $P < 0.05$).

Table 5
Visual score of DNA damage in tumor cell lines treated with compounds **5**, **11** and **15**.

Treatment	No. of cells		Class**				DNA damaged cells % (Mean ± SEM)
	Analyzed*	Comets	0	1	2	3	
Control (-ve)	400	45	355	34	9	2	11.25 ± 0.75[c]
Control (+ve)	400	94	306	41	34	19	23.50 ± 0.29 [a]
Sample 5	400	65	335	38	19	8	16.25 ± 0.48[b]
Sample 11	400	79	321	42	21	16	19.75 ± 0.49[ab]
Sample 15	400	68	332	41	19	8	17.00 ± 0.41[b]

* : Number of cells examined per a group,
** : Class 0 = no tail; 1 = tail length < diameter of nucleus; 2 = tail length between 1X and 2X the diameter of nucleus; and 3 = tail length > 2X the diameter of nucleus.

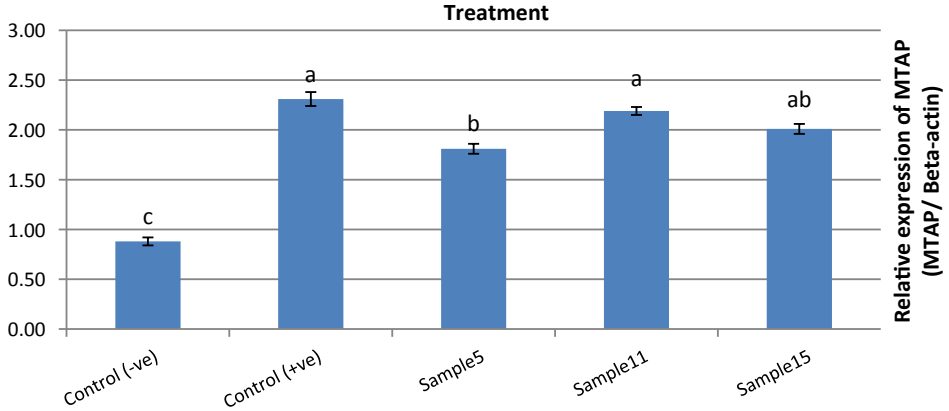

Fig. 2. The alterations of MTAP gene in tumor cell lines treated with tested compounds Data are presented as mean ± SEM. [a–c]Mean values within tissue with unlike superscript letters were significantly different ([a:] $P < 0.01$, [b and c] $P < 0.05$).

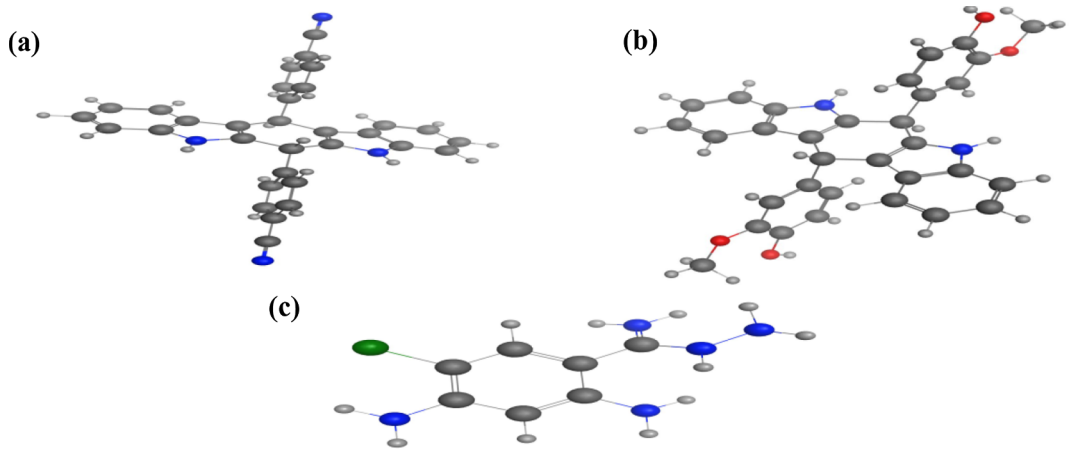

Fig. 4. Lowest energy conformers of most active compounds (a) 11 (b) 15 and reference compound (c) Amiloride with balls and cylinders rendering.

deeper location into the cavity which may lead to a higher binding interaction within the hydrophobic residues in the uPA active site and hence attribute its higher activity pattern. (Fig. 8).

2.5.2. Surface mapping

In a valuable research for reasons behind the activity of compounds under investigation, hydrophobic surface mapping study was performed. As there is a powerful link between hydrophobicity and effective binding to uPA [31]. Compounds **11** and **15** clearly showed a preference for more hydrophobic regions (more greener areas on the map, Fig. 9a and b that could be attributed to the presence of two indole ring in addition to phenyl moieties in both compounds causing higher lipophilic character of the whole molecule even more than the reference modeling compound amiloride Fig. 9c.

3. Conclusion

The current research paper was directed towards breast cancer targeting via the synthesis of some new tetrahydroindolocarbazoles derivatives **(1–20)**. The results revealed that compounds **11**, **15** and **5** possessed the higher cytotoxicity on breast (MCF-7) human tumor cell line with LC_{50} 5.7, 10.8, 33.1 respectively. By measuring the level of uPA protein expression for the most active tested compounds **11** and **15** the results indicated that they may exert their anticancer activity by inhibiting uPA and possess significant anticancer activity comparable to the activity of the commonly used anticancer drug, doxorubicin. Gene expression analysis by Quantitative Real Time PCR and DNA damage assay were performed for the active derivatives, results supported the higher activity of tested compounds. Molecular docking study of the present work revealed that active uPA inhibitors candidates **11** and **15** bound with similar amino acid residues as amiloride especially mentioning Arg 217 and Gly 216 which support our hypothesis that these compounds could exert their antibreast cancer activity action *via* uPA inhibition. Surface mapping has illustrated active candidates under study showed good binding to uPA by having optimal lipophilicity required for effective binding. Thus this work presents two active antibreast cancer candidates **11** and **15.** More studies will be conducted for further optimization of active derivatives to be drug candidates.

4. Experimental section

The melting points were measured on a Boetius-Mikroheiztisch the company “VEB weighing, Rapido Radebeul/VEB NAGEMA” measured and are uncorrected. The carbon, hydrogen and nitrogen content of the substances were performed on a “CHNS-932” automatic analyzer of the company “LECO Corporation” in the automatic Micro chemical determined. The halogen content was determined by titration in semi micro method determined. For the analyzes TLC were with aluminium foil fluorescent indicator from Merck KGaA (silica gel 60 F254, layer thickness 0.2 mm) used. Rf -values (run level relative to the solvent front), The separations were with column chromatography at atmospheric pressure on silica gel 60 (Grain size from 0.063 to 0.200 mm) from Merck KGaA. The NMR spectra were recorded on a “Gemini 2000” (400/100 MHz). The ATR spectrawere recorded on an FT-IR spectrometer “IFS 28” by “Bruker”, the KBr spectra on an FT-IR Spectrometer “Spectrum BX” the Company “PerkineElmer” measured. The ESI mass

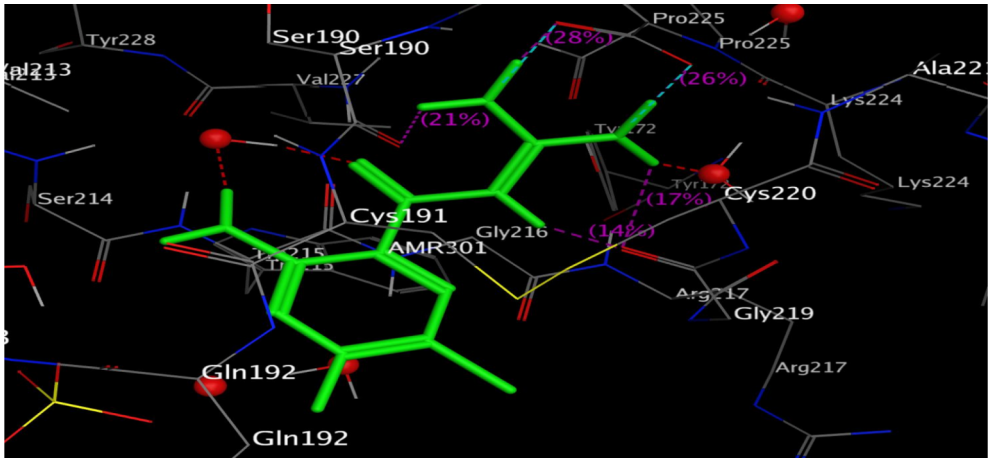

Fig. 5. The 3D binding mode and residues involved in the recognition for Amiloride The hydrogen bonding were represented as pink dotted lines.

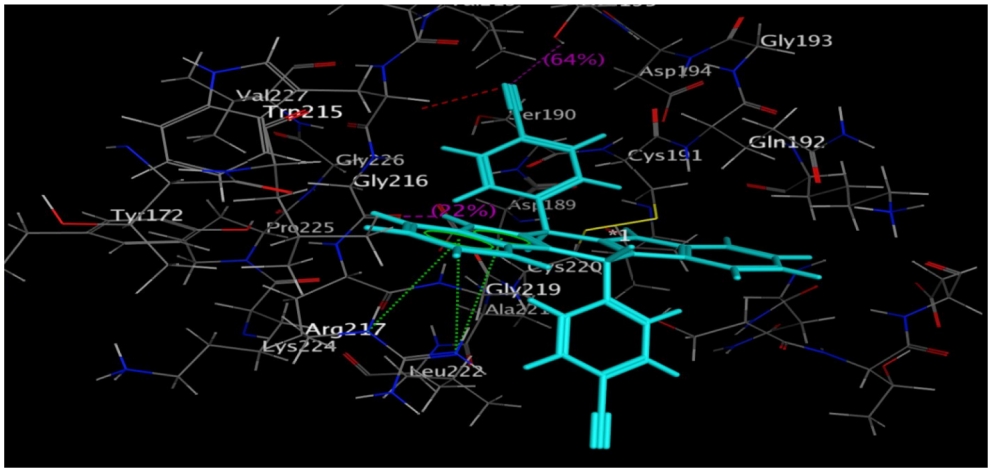

Fig. 6. The 3D binding mode and residues involved in the recognition for compound 11. The hydrogen bonding residues at the binding site are tagged in dotted lines.

spectra were recorded on a "Finnigan LCQ Classic" by "thermal Electron measured" the sample was injected directly.

4.1. Chemistry

4.1.1. General procedure for the preparation of THICZs (1 – 20)

0.002 mol of substituted aromatic aldehyde were added to a stirred methanolic solution of 0.002 mol of indole or its derivative till complete dissolution. Catalytic amount of concentrated H_2SO_4 were added while stirring. Reflux the mixture for additional 1 hr. The completion of the reaction was monitored by TLC (100% CH_2Cl_2). The reaction was then terminated by addition of 50 ml of water followed by neutralization with NH_4OH solution. The product was then extracted twice by ethylacetate, washed with water, and finally dried over anhydrous Na_2SO_4. The obtained filterate is concentrated under vacuum and the crude product was purified *via* column chromatography on silica gel using (30% EtAc/hexane) as a solvent to afford the target THICZs derivatives **1–20**. The THICZs (**1–8** and **18–20**) were previously reported and their identities are equivalent to the synthesized samples, whereas the THICZs (**9–17**) new derivatives were confirmed by the means of ^{1}H- and ^{13}C NMR, ESI-MS and IR spectra (see supporting information).

4.1.2. 6,12-bis(4-(benzyloxy)-3-methoxyphenyl)-5,6,11,12-tetrahydroindolo[3,2-b]carbazole (9)

White powder, Mp 282–284 °C, yield 86%, $C_{46}H_{38}N_2O_4$, 682.80 g/mol, ESI-MS: 683.30 [M + H^+], IR (ATR,cm-1): 3368(NH), ^{1}H NMR (400 MHz, DMSO-d_6): δ (ppm) = 3.83 (s, 6H, 2OCH_3), 4.94 (s, 4H, 2OCH_2), 5.54 (s, 2H, 2CH), 6.71 (dd, 2H, J = 1.9, 8.6 Hz, ArH), 6.81 (s, 2H, ArH), 6.96 (d, 4H, J = 7.2 Hz, ArH), 7.17–7.21 (m, 14H, ArH), 7.30 (dd, 2H, J = 2.0, 7.5 Hz, ArH), 10.31 (s, 2H, 2NH), ^{13}C NMR (100 MHz,acetone-d_6) δ (ppm): 29.2 (CH), 30.6 (CH), 55.5 (OCH_3), 56.00 (OCH_3), 74.1 (OCH_2), 76.1 (OCH_2), 109.0–148.1 (40C, Aromatic-C), EA calcd. C, 80.92, H, 5.61, N, 4.10, found C, 80.91, H, 5.60, N, 4.11, Rf 0.79 (CH_2Cl_2).

4.1.3. 6,12-bis(4-methoxyphenyl)-5,6,11,12-tetrahydroindolo[3,2-b] carbazole (10)

Yellow powder, mp. 146–147 °C, yield 56%, 470.56 g/mol, $C_{32}H_{26}N_2O_2$, ESI-MS: 471.22 [M + H^+], IR (ATR,cm^{-1}): 3802 (NH), 2989, 2990 (CH), ^{1}H NMR (400 MHz, DMSO-d_6): δ (ppm): 3.71 (s, 3H, OCH_3), 3.80 (s, 3H, OCH_3), 5.43 (s, 2H, 2CH), 7.32 (t, 4H, J = 7.8 Hz, ArH), 7.51(d, 2H, J = 8.0 Hz, ArH), 7.44 (d, 2H, J = 8.0 Hz, ArH), 7.65–7.71 (m, 4H, ArH), 7.91 (d, 2H, J = 7.5 Hz, ArH), 8.02–8.11 (m, 2H, ArH), 9.88 (s, 1H, 1NH), 10.14 (s, 1H, 1NH). ^{13}C NMR: (100 MHz, DMSO-d_6) δ (ppm) = 45.1 (CH), 47.0 (CH), 55.6 (OCH_3), 56.7 (OCH_3), 111.0–137.3 (28C, Aromatic-C), EA calcd. : C, 81.68, H, 5.57, N, 5.95, found C, 81.66, H, 5.58, N, 5.93, R$_f$ 0.55 (CH_2Cl_2).

4.1.4. 4,4′-(5,6,11,12-tetrahydroindolo[3,2-b]carbazole-6,12-diyl) dibenzonitrile (11)

Yellow crystals, mp. 138–139 °C, yield 76%, 460.53 g/mol, $C_{32}H_{20}N_4$, ESI-MS: 461.11 [M + H^+], IR (ATR, cm^{-1}): 3865 (NH), 2994, 2999 (CH), ^{1}H NMR (400 MHz, DMSO-d_6): δ (ppm): 5.53 (s, 2H, 2CH), 6.82–6.84 (m, 2H, ArH), 7.12 (t, 4H, J = 7.8 Hz, ArH), 7.41(d, 2H, J = 8.0 Hz, ArH), 7.54 (d, 4H, J = 8.0 Hz, ArH), 7.56–7.57 (m, 4H, ArH), 10.45 (s, 1H, 1NH), 10.56 (s, 1H, 1NH), ^{13}C NMR: (100 MHz,

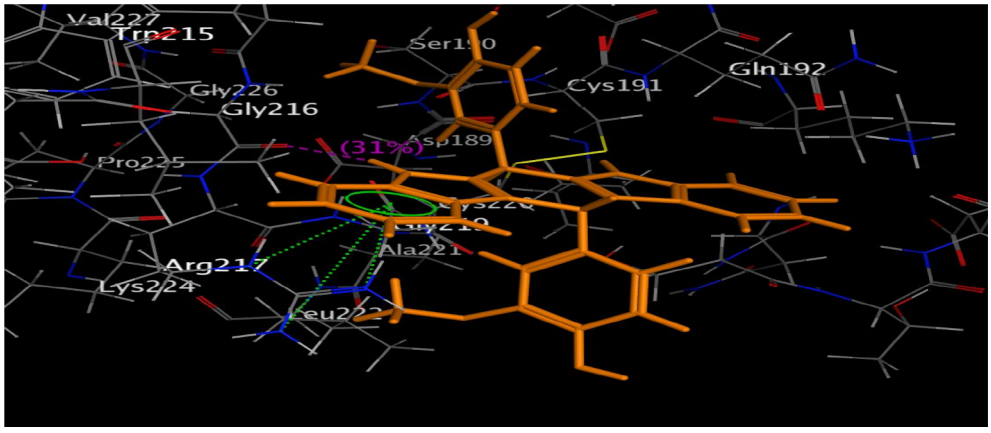

Fig. 7. The 3D binding mode and residues involved in the recognition for compound 15. The hydrogen bonding residues at the binding site are tagged in dotted lines.

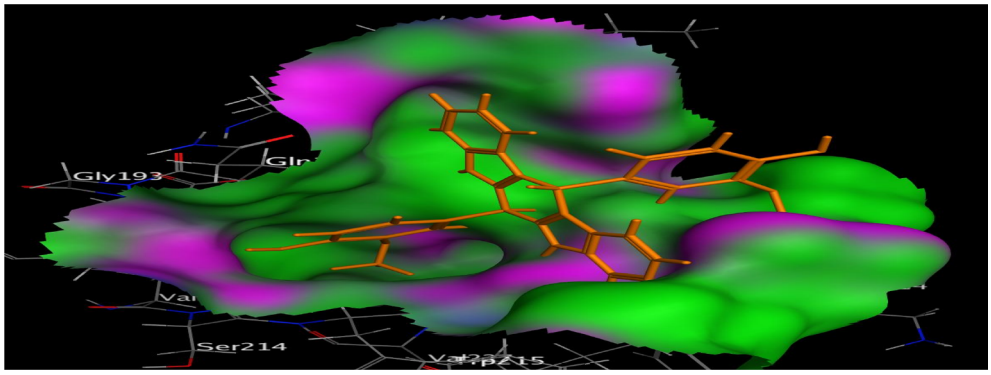

Fig. 8. Overelay of compound 15 embedded into the surface mapping pocket Pink: hydrogen bond, blue: mild polar, green: hydrophobic region.

DMSO-d_6) δ (ppm) = 45.1 (CH), 47.0 (CH), 111.0 (CN), 118.7 – 144.3 (29 C, Aromatic-C), EA calcd. : C, 83.46, H, 4.38, N, 12.17, found C, 83.47, H, 4.39, N, 12.16, R_f 0.45 (CH_2Cl_2).

4.1.5. 6,12-bis(2,4-dinitrophenyl)-5,6,11,12-tetrahydroindolo[3,2-b] carbazole (12)

Yellow powder, Mp 232–234 °C, yield 66%, $C_{30}H_{18}N_6O_8$, 590.50 g/mol, ESI-MS: 591.11 [M + H^+], IR (ATR, cm^{-1}): 3388(NH), ^{1}H NMR (400 MHz, DMSO-d_6): δ (ppm) = 5.43 (s, 2H, 2CH), 6.57 (dd, 2H, J = 1.9, 8.6 Hz, ArH), 6.83 (s, 2H, Ar-H), 7.23 (t, 4H, J = 7.2 Hz, ArH), 7.47–7.49 (m, 4H, ArH), 7.60 (dd, 2H, J 2, 7.5 Hz, ArH), 10.34 (s, 2H, 2NH), ^{13}CNMR (100 MHz,acetone-d_6) δ (ppm): 30.55 (CH), 32.5 (CH), 109.1–150.2 (28C, Aromatic-C), EA calcd. C, 61.02, H, 3.07, N, 14.23, found C, 61.02, H, 3.06, N, 14.22, R*f* 0.29 (CH_2Cl_2).

4.1.6. 6,12-bis(2,6-dinitrophenyl)-5,6,11,12-tetrahydroindolo[3,2-b] carbazole (13)

Pale yellow powder, Mp 222–224 °C, yield 58%, $C_{30}H_{18}N_6O_8$, 590.50 g/mol, ESI-MS: 591.15 [M + H^+], IR (ATR, cm^{-1}): 3398(NH), ^{1}H NMR (400 MHz, DMSO-d_6): δ (ppm) = 5.44 (s, 2H, 2CH), 7.21 (d, 4H, J = 7.2 Hz, ArH), 7.45–7.47 (m, 6H, ArH), 7.63 (t, 4H, J = 7.5 Hz, ArH), 10.51 (s, 2H, 2NH), ^{13}CNMR (100 MHz, acetone-d_6) δ (ppm): 32.51 (CH), 35.4 (CH), 108.1–150.9 (28C, Aromatic-C), EA calcd. C, 61.02, H, 3.07, N, 14.23, found C, 61.03, H, 3.08, N, 14.21, R*f* 0.19 (CH_2Cl_2).

4.1.7. 6,12-bis(3-methoxyphenyl)-5,6,11,12-tetrahydroindolo[3,2-b] carbazole (14)

Yellow orange powder, mp. 166–167 °C, yield 75%, 470.56 g/mol, $C_{32}H_{26}N_2O_2$, ESI-MS: 471.15 [M + H^+], IR (ATR, cm^{-1}): 3822 (NH), 2988, 2994 (CH), ^{1}H NMR (400 MHz, DMSO-d_6): δ (ppm): 3.72 (s, 3H, OCH_3), 3.85 (s, 3H, OCH_3), 5.46 (s, 2H, 2CH), 6.44 (s, 2H, ArH), 7.34 (t, 4H, J = 7.8 Hz, ArH), 7.42(d, 2H, J = 8.0 Hz, ArH), 7.46 (d, 2H, J = 8.0 Hz, ArH), 7.57–7.59 (m, 4H, ArH), 7.90 (d, 2H, J = 7.5 Hz, ArH), 9.98 (s, 1H, 1NH), 10.33 (s, 1H, 1NH), ^{13}C NMR: (100 MHz, DMSO-d_6) δ (ppm) = 43.1 (CH), 45.0 (CH), 55.7 (OCH_3), 58.1 (OCH_3), 112.0 – 142.6 (28C, Aromatic-C). EA calcd. : C, 81.68, H, 5.57, N, 5.95, found C, 81.69, H, 5.59, N, 5.94, R_f 0.75 (CH_2Cl_2).

4.1.8. 4,4′-(5,6,11,12-tetrahydroindolo[3,2-b]carbazole-6,12-diyl)bis(2-methoxyphenol) (15)

Yellow powder, mp. 166–167 °C, yield 75%, 502.56 g/mol, $C_{32}H_{26}N_2O_4$, ESI-MS: 503.81 [M + H^+], IR (ATR, cm^{-1}): 3842 (NH), ^{1}H NMR (400 MHz, DMSO-d_6): δ (ppm): 3.78 (s, 6H, OCH_3), 5.66 (s, 2H, 2CH), 7.40 (t, 4H, J = 7.0 Hz, ArH), 7.45 (d, 2H, J = 9.0 Hz, ArH), 7.46 (d, 2H, J = 8.8 Hz, ArH), 7.52 (s, 2H, ArH), 7.90 (d, 4H, J = 7.0 Hz, ArH), 10.01 (s, 2H, 2OH), 10.35 (s, 2H, 2NH), ^{13}C NMR: (100 MHz, DMSO-d_6) δ (ppm) = 44.32 (CH), 45.20 (CH), 56.4 (OCH_3), 60.06 (OCH_3), 110.0–152.9 (28C, Aromatic-C). EA calcd.: C, 76.48, H, 5.21, N, 5.57 found C, 76.49, H, 5.20, N, 5.56, R_f 0.45 (CH_2Cl_2).

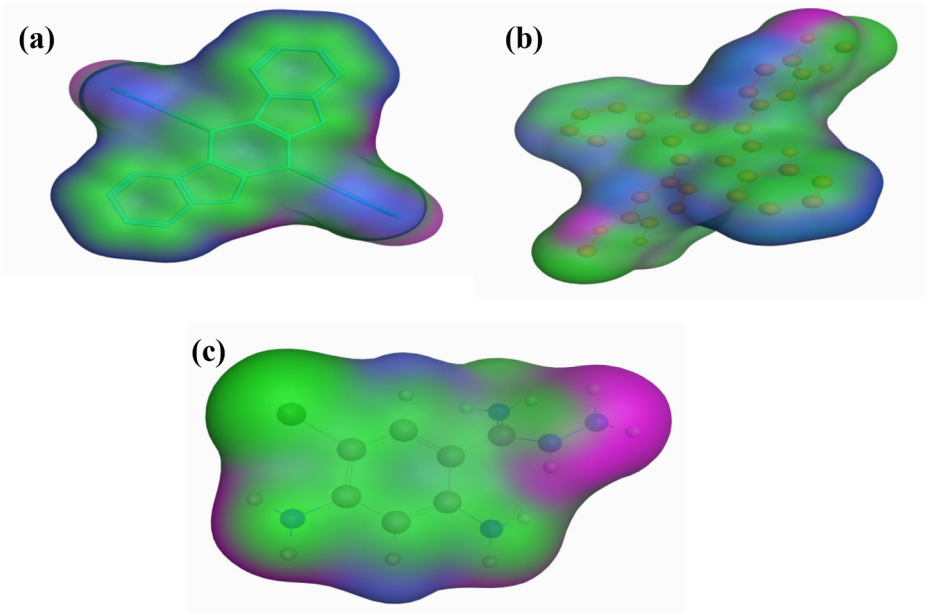

Fig. 9. Surface map for (a) the most active compound 11; (b) Compound 15, (c) Amiloride Pink: hydrogen bond, blue: mild polar, green: hydrophobic region.

4.1.9. 2,2′-(5,6,11,12-tetrahydroindolo[3,2-b]carbazole-6,12-diyl) dibenzene-1,4-diol (16)

Yellow powder, mp. 162–163 °C, yield 75%, 474.51 g/mol, $C_{30}H_{22}N_2O_4$, ESI-MS: 475.15 [M + H^+], IR (ATR, cm^{-1}): 3822 (br. OH and NH), 2988, 2994 (CH), ^{1}H NMR (400 MHz, DMSO-d_6): δ (ppm): 5.52 (s, 2H, 2CH), 6.46 (s, 2H, ArH), 7.35 (t, 4H, J = 7.4 Hz, ArH), 7.43 (d, 2H, J = 7.8 Hz, ArH), 7.51 (d, 2H, J = 7.5 Hz, ArH), 7.58–7.06 (m, 2H, ArH), 7.78 (d, 2H, J = 8.0 Hz, ArH), 9.88 (brs, 2H, 2OH), 10.12 (brs, 2H, 2OH), 10.26 (s, 2H, 2NH). ^{13}C NMR: (100 MHz, DMSO-d_6)δ (ppm) = 44.12 (CH), 46.11 (CH), 111.0 – 152.0 (28C, Aromatic-C). EA calcd.: C, 75.94, H, 4.67, N, 5.90, found C, 75.95, H, 4.68, N, 5.91, R_f 0.49 (CH_2Cl_2).

4.1.10. 6,12-bis(4-(benzyloxy)phenyl)-5,6,11,12-tetrahydroindolo[3,2-b] carbazole (17)

Light green fine powder, Mp 200–202 °C, yield 85%, $C_{44}H_{34}N_2O_2$, 622.75 g/ mol, ESI-MS: 623.26 [M + H^+], 621.31 [M − H^+], IR (ATR, cm^{-1}) 3396 (NH), ^{1}H NMR (400 MHz, DMSO-d_6): δ (ppm): 5.03 (s, 4H, $2CH_2O$), 5.60 (s, 2H, 2CH), 6.82 (t, 4H, J = 7.3 Hz, ArH), 6.99 (d, 4H, J = 7.9 Hz, ArH), 7.02 (d, 4H, J = 7.2 Hz, ArH), 7.03 (d, 4H, J = 7.7 Hz, ArH), 7.32 –7.38 (m, 5H, ArH), 7.43–7.49 (m, 5H, ArH), 10.88 (s, 2H, 2NH). ^{13}C NMR (100 MHz, DMSO-d_6): δ (ppm): 36.7 (CH), 40.8 (CH), 69.6 (OCH_2), 74.0 (OCH_2), 110.4–157.4 (40C, Aromatic-C), EA calcd. C, 84.86; H, 5.50; N, 4.50, found C, 84.87, H, 5.52, N, 4.49, R_f 0.73 (CH_2Cl_2).

4.2. Antitumor screening

Human breast carcinoma (MCF-7 cell line) was used in the biological assay and they were obtained from Vacsera (Giza, Egypt). Cell cultures procedures were performed in a sterile area using a laminar air flow cabinet biosafety class II level. Culture was maintained in DMEM F12 medium with 1% antibiotic-antimycotic mixture (10,000 U/ml potassium penicillin, 10,000 µg/ml streptomycin sulfate and 25 µg/ml amphotericin B), 1% L-glutamine, and supplemented with 10% heat inactivated fetal bovine serum. Culturing and subculturing were carried out according to the reported procedure. A negative control composed of DMSO was also used [17]. Cell viability assay were conducted according to reported method [18,19]. Following culturing for 10 days, the cells were seeded at concentration of 10×10^3 cells per well in a fresh complete growth medium using 96-well microtiter plastic plates at 37 °C for 48 h under 5% CO_2, in a water jacketed carbon dioxide incubator. Fresh medium (without serum) was added and cells were incubated either alone (negative control) or with Samples to give a final concentration of 100 µg/ml. After 24 h incubation, the medium was aspirated and then 40 µl MTT salt (2.5 mg/ml) were added to each well and incubated for further four hours at 37 °C under 5% CO2. To stop the reaction and dissolve the formed crystals, 200 µl 10% sodium dodecyl sulphate (SDS) in deionized water was added to each well and incubated overnight at 37 °C. The absorbance was measured using a microplate multi-well reader at 595 nm and a reference wavelength of 690 nm. Cell viability was assessed according to the mitochondrial-dependent reduction of yellow MTT (3-(4, 5-dimethylthiazol-2-yl)-2, 5-diphenyl tetrazolium bromide) to purple formazan.

4.3. Urokinase inhibition assays

According to the manufacturer's instructions, after 24 h from treatment of the cells with IC_{50} values of each compound, medium was collected and centrifuged at 2000 xg for 10 min to remove cellular debris. Add 50 µl of the cell extract per well and incubate for 2 h. Wells were washed with 200 µl of wash buffer then add 50 µl of biotinylated uPA antibody to each well and incubate for 1 h at 25 °C. After washing, plates were incubated with 50 µl of streptavidin-peroxidase conjugate per well and incubate for 30 min then wash the microplate as described above. Add 50 µl of chromogen substrate per well and incubate for about 10 min or till the optimal blue color density develops. Add 50 µl of stop solution to each well. The color will change from blue to yellow. Read the absorbance on a microplate reader at a wavelength of 450 nm immediately. The concentrations of uPA in the samples were determined based on the uPA standard curve.

4.4. Molecular genetics

4.4.1. Quantitative real time- PCR (qPCR)

Total RNA was isolated from tumor cell lines using the RNeasy Mini Kit (Qiagen, Hilden, Germany) supplemented with DNaseI (Qiagen) digestion step, according to the manufacturer's protocol. Isolated total RNA was treated with one unit of RQ1 RNAse-free DNAse (Invitrogen, Germany) to digest DNA residues, re-suspended in DEPC-treated water and quantified photospectrometrically at 260 nm. Purity of total RNA was assessed by the 260/280 nm ratio which was between 1.8 and 2.1. Additionally, integrity was assured with ethidium bromide-stain analysis of 28 S and 18 S bands by formaldehyde-containing agarose gel electrophoresis. Aliquots were used immediately for reverse transcription (RT), otherwise they were stored at −80 °C. Complete Poly(A)$^+$ RNA isolated from tumor cell lines was reverse transcribed into cDNA in a total volume of 20 µl using RevertAid™ First Strand cDNA Synthesis Kit (Fermentas, Germany). An amount of total RNA (5 µg) was used with a master mix. The master mix was consisted of 50 mM $MgCl_2$, 10 × RT buffer (50 mM KCl; 10 mM Tris-HCl; pH 8.3), 10 mM of each dNTP, 50 µM oligo-dT primer, 20 IU ribonuclease inhibitor (50 kDa recombinant enzyme to inhibit RNase activity) and 50 IU MuLV reverse transcriptase. The mixture of each sample was centrifuged for 30 s at 1000 g and transferred to the thermocycler. The RT reaction was carried out at 25 °C for 10 min, followed by 1 h at 42 °C, and finished with a denaturation step at 99 °C for 5 min. Afterwards the reaction tubes containing RT preparations were flash-cooled in an ice chamber until being used for cDNA amplification through quantitative Real Time-polymerase chain reaction (qRT-PCR). Step One™ Real-Time PCR System from Applied Biosystems (Thermo Fisher Scientific, Waltham, MA USA) was used to determine the tumor cell lines cDNA copy number. PCR reactions were set up in 25 µl reaction mixtures containing 12.5 µl 1 × SYBR® Premix Ex TaqTM (TaKaRa, Biotech. Co. Ltd.), 0.5 µl 0.2 µM sense primer, 0.5 µl 0.2 µM antisense primer, 6.5 µl distilled water, and 5 µl of cDNA template. The reaction program was allocated to 3 steps. First step was at 95.0 °C for 3 min. Second step consisted of 40 cycles in which each cycle divided to 3 steps: (a) at 95.0 °C for 15 *sec*; (b) at 55.0 °C for 30 *sec*; and (c) at 72.0 °C for 30 *sec*. The third step consisted of 71 cycles which started at 60.0 °C and then increased about 0.5 °C every 10 *sec* up to 95.0 °C. At the end of each sqRT-PCR a melting curve analysis was performed at 95.0 °C to check the quality of the used primers. Each experiment included a distilled water control. The sequences of specific primer of the genes used are listed in Table 4. At the end of each qPCR a melting curve analysis was performed at 95.0 °C to check the quality of the used primers. The relative quantification of the target to the reference was determined by using the $2^{-\Delta\Delta CT}$ method as follows:

$$\Delta C_{T(test)} = C_{T(target,\ test)} - C_{T(reference,\ test)},$$
$$\Delta CT(calibrator) = C_{T(target,\ calibrator)} - C_{T(reference,\ calibrator)},$$
$$\Delta\Delta CT = \Delta C_{T(Test)} - \Delta C_{T(calibrator)}.$$

4.4.2. DNA damage using the comet assay

The neutral comet assay for tumor cell lines was used as described according to the reported protocol [26,27]. After the trypsin treatment to produce a single cell suspension, approximately 1.5×10^4 cells were embedded in 0.75% low-gelling-temperature agarose and rapidly pipetted onto a pre-coated microscope slide. Samples were lysed for 4 h at 50 °C in 0.5% SDS, 30 mM EDTA, pH 8.0. After rinsing overnight at room temperature in Tris/borate/EDTA buffer, pH 8.0, samples were electro-phoresed for 25 min at 0.6 V/cm, and then stained with

propidium iodide. Slides were viewed using a fluorescence microscope with a CCD camera, and 150 individual comet images were analyzed from each sample for tail moment, DNA content, and percentage DNA in tail. For each sample about 100 cells were examined to determine the percentage of cells with DNA damage that appear like comets. The nonoverlapping cells were randomly selected and were visually assigned a score on an arbitrary scale of 0–3 (i.e., class 0 = no detectable DNA damage and no tail; class 1 = tail with a length less than the diameter of the nucleus; class 2 = tail with length between 1 × and 2 × the nuclear diameter; and class 3 = tail longer than 2 × the diameter of the nucleus) based on perceived comet tail length migration and relative proportion of DNA in the nucleus.

4.5. Molecular modelling

The coordinates of (PDB ID: 1f51) for docking calculations was obtained from the Brookhaven Protein Data Bank. Ligands under study were drawn using MOE 2D sketcher Then energy minimization was computed Protein was prepared using the MOE 10.9 Water molecules which are important in aiding the interaction with the receptor were optimized Lowest energy aligned conformation(s) were identified. This corrected protein structure was used in the subsequent docking studies. Moreover addition of Hydrogen atoms at their standard geometry, then computing the partial charges followed by energy optimization. Scoring function was conducted by the aid of triangle matcher as placement method also affinity dG was validated for docking. The retention of 30 conformers with the highest and best score was employed. Amiloride as areference drug was docked into the active site. The active site has been defined. All atoms located less than 10.0 A° from any ligand atom were considered. Surgace mapping calculations were performed by 'Molecular Operating Environment' software (MOE of Chemical Computing Group Inc., on a Core i7, 2.3 GHz workstation) [32–36].

Declaration of Competing Interest

The authors declare that they have no known competing financial interests or personal relationships that could have appeared to influence the work reported in this paper.

Appendix A. Supplementary material

Supplementary data to this article can be found online at https://doi.org/10.1016/j.bioorg.2019.103332.

References

[1] B. Degryse, The urokinase receptor system as strategic therapeutic target: challenge for the 21st century, Curr. Pharma. Des. 17 (2011) 11872–11873.
[2] L. Tang, X. Han, The urokinase plasminogen activator system in breast cancer invasion and metastasis, Biomed. Pharmacothe. 67 (2013) 179–182.
[3] J. Jankun, E. Skrzypczak-Jankun, Molecular basis of specific inhibition of urokinase plasminogen activator by amiloride, Cancer Biochem. Biophys. 17 (1999) 109–123.
[4] H. Matthews, M. Ranson, M. Kelso, Anti-tumour/metastasis effects of the potassium-sparing diuretic amiloride: an orally active anti-cancer drug waiting for its call-of-duty? Int. J. Cancer. 129 (2011) 2051–2061.
[5] W.M. Eldehnaa, H. Almahlia, G.H. Al-Ansary, H.A. Ghabbourd, M.H. Alye, O. Ismael, A. Al-Dhfyan, H.A. Abdel-Aziz, Synthesis and in vitro anti-proliferative activity of some novel isatins conjugated with quinazoline/phthalazine hydrazines against triple-negative breast cancer MDA-MB-231 cells as apoptosis-inducing agents, J. Enzyme Inhib. Med. Chem. 32 (1) (2017) 600–613.
[6] E. Zeslawska, A. Schweinitz, A. Karcher, P. Sondermann, S. Sperl, J. Sturzebecher, U. Jacob, Crystals of the urokinase type plasminogen activator variant βc-uPA in complex with small molecule inhibitors open the way towards structure-based drug design, J. Mol. Bio. 301 (2000) 465–475.
[7] M.J. Duffy, Urokinase plasminogen activator, its inhibitor, PAI-1, as prognostic markers in breast cancer; from pilot to level 1 evidence studies, Clin. Chem. 48 (2002) 1194–1197.
[8] F. Descotes, B. Riche, G. De Saez, J. Laroche, P. Roy Datchary, et al., Plasminogen activator inhibitor type 1 is the most significant of the usual tissue prognostic factors in node-negative breast ductal adenocarcinoma independent of urokinase-type plasminogen activator, Clin. Breast Cancer 8 (2008) 168–177.
[9] N. Harbeck, M. Schmitt, R.E. Kates, M. Kiechle, I. Zemzoum, F. Janicke, et al., Clinical utility of urokinase-type plasminogen activator and plasminogen activator inhibitor-1 determination in primary breast cancer tissue for individualized therapy concepts, Clin. Breast Cancer 3 (2002) 196–200.
[10] (a) M.T. El Sayed, N.A. Hamdy, D.A. Osman, Indoles as anti-cancer agents, Adv. Mod. Oncol. Res. 1 (2015) 20–35;
(b) M.T. El Sayed, K.M. Ahmed, K. Mahmoud, A. Hilgeroth, Synthesis, cytostatic evaluation and structure activity relationships of novel bis-indolylmethanes and their corresponding tetrahydroindolocarbazoles, Eur. J. Med. Chem. 90 (2015) 845–859.
[11] (a) S. Dadashpour, S. Emami, Indole in the target-based design of anticancer agents: a versatile scaffold with diverse mechanisms, Euro. J. Med. Chem. 150 (2018) 9–29;
(b) J.S. Sidhu, R. Singla, M. Sharma, Indole derivatives as anticancer agents for breast cancer therapy: a review, Anti-Cancer Agents Med. Chem. (Form. Curr. Med. Chem. - Anti-Cancer Agents) (2015).
[12] M.T. El Sayed, A. Voronkov, I. Ogungbe, S.M. El-Hallouty, K.M. Ahmed, B. Vladimir, K. Balakin, Anti-cancer, molecular docking and structure activity relationship studies of some novel synthetic spiroindolo[3,2-*b*]carbazoles as predicted HER2 and BrK kinase inhibitors, Curr. Bioactive Comp. 13 (2017) 10.2174/1573407213666170213154357.
[13] (a) M.T. El Sayed, H.A.R. Hussein, K.M. Ahmed, Synthesis and antiproliferative activity of some novel indole Mannich bases, Adv. Mod. Oncol. Res. 1 (2015) 104–111;
(b) M. El-Sharief, M.H. El-Naggar, E.M. Ahmed, S.M. El-Messery, A.E. Mahmoud, M.M. Alif, L.M. Salemg, K.F. Mahrousg, M.T. El Sayed, Tetrahydroindolocarbazoles (THICZs) as new class of urokinase (uPA) inhibitors: synthesis, anticancer evaluation, DNA-damage determination, and molecular modelling study, Bioorgan. Chem. 80 (2018) 545–554.
[14] D. Maciejewska, I. Szpakowska, I. Wolska, M. Niemyjska, M. Mascini, M. Maj-Zurawska, DNA-based electrochemical biosensors for monitoring of bis-indoles as potential antitumoral agents, chemistry, X-ray crystallography, Bioelectrochemistry 69 (2006) 1–9.
[15] D. Maciejewska, I. Wolska, M. Niemyjska, P. Zero, Structure in solid state of 3,3′-diindolylmethane derivatives, potent cytotoxic agents against human tumor cells, followed X-ray diffraction and 13C CP/MAS NMR analyses, J. Mol. Struct. 753 (2005) 53–60.
[16] G.D. Stoner, H. Mukhtar, Polyphenols as cancer chemopreventive agents, J. Cell. Biochem. 22 (1995) 169–180.
[17] M. Thabrew, R.D. Hughes, I.G. Mcfarlane, Screening of hepatoprotective plant components using a HepG2 cell cytotoxicity assay, J. Pharm. Pharmacol. 49 (1997) 1132–1135.
[18] S.M. Moustafa, B.M. Menshawi, G.M. Wassel, M.M. Mounier, Screening of some plants in Egypt for their cytotoxicity against four human cancer cell lines, Int J chemtech Res 6 (2014) 1074–1084.
[19] T. Mosmann, Rapid colorimetric assay for cellular growth and survival: application to proliferation and cytotoxicity assays, J. Immunol. Meth. 65 (1983) 55–63.
[20] G. Markus, S. Camiolo, S. Kohga, J. Madeja, A. Mittleman, Plasminogen activator secretion of human tumors in short-term organ culture, including a comparison of primary and metastatic colon tumors, Cancer Res. 43 (1983) 5517–5525.
[21] J. Unkeless, K. Dang, G. Kellerman, E. Reich, Fibrinolysis associated with oncogenic transformation, J. Biol. Chem. 249 (1974) 4295–4305.
[22] S. Siicela, J. Barrett, In vitro degradation of radiolabelled, intact basement membrane mediated by cellular plasminogen activator, Carcinogenesis (Lond.) 3 (1982) 363–369.
[23] S. Ulisse, E. Baldini, S. Sorrenti, M. D'Armiento, The urokinase plasminogen activator system: a target for anti-cancer therapy, Curr. Cancer Drug Targets 9 (2009) 32–71.
[24] L. Gutierrez, A. Schulman, T. Brito-Robinson, F. Noria, V.A. Ploplis, F.J. Castellino, Tumor development is retarted in mice lacking the gene for urokinase-type plasminogen activator or its inhibitor, plasminogen activator inhibitor-1, Cancer Res. 60 (2000) 5839–5847.
[25] M.A. Omar, Y.M. Shaker, S.A. Galal, M.M. Ali, S.M. Kerwin, J. Li, H. Tokuda, R.A. Ramadan, H.I. El Diwani, Synthesis and docking studies of novel antitumor benzimidazoles, Bioorg. Med. Chem. 20 (2012) 6989–7001.
[26] S.F. De Oliveira, M. Ganzinelli, R. Chilà, L. Serino, M.E. Maciel, Urban C. de Andrade, R.S. De Lima, I.J. Cavalli, D. Generali, M. Broggini, G. Damia, Characterization of MTAP gene expression in breast cancer patients and cell lines, PLoS One 11 (1) (2016) e0145647.
[27] P.L. Olive, J.P. Banáth, R.E. Durand, Heterogeneity in radiation-induced DNA damage and repair in tumor and normal cells measured using the "comet" assay. 1990, Radiat. Res. 178 (2012) AV35-42.
[28] C.S. Gondi, S.S. Lakka, D.H. Dinh, W.C. Olivero, M. Gujrati, J.S. Rao, Intraperitoneal injection of a hairpin RNA—expressing plasmid targeting urokinase-type plasminogen activator (uPA) receptor and uPA retards angiogenesis and inhibits intracranial tumor growth in nude mice, Clin. Cancer Res. 13 (2007) 4051–4060.
[29] V. Hofmeister, D. Schrama, J.C. Becker, Anti-cancer therapies targeting the tumor stroma, Cancer Immunol. Immunother. 57 (2008) 1–17.
[30] Y. Li, P.J. Cozzi, Targeting uPA/uPAR in prostate cancer, Cancer Treatm. Rev. 33 (2007) 521–527.
[31] C. De Bock, Y. Wang, Clinical significance of urokinase-type plasminogen activator receptor (uPAR) expression in cancer, Med. Res. Rev. 24 (2004) 13–39.
[32] M. Feher, E. Sourial, J.M. Schmidt, P. Labute, et al., Flexible alignment of small molecules, J. Med. Chem. 44 (2001) 1483–1490.
[33] V. Cody, C.H. Schwalbe, Structural characteristics of antifolate dihydrofolate reductase enzyme interactions, Crystallogr. Rev. 12 (2006) 301–333.
[34] J.P. Volpato, B.J. Yachnin, J. Blanchet, V. Guerrero, L. Poulin, E.A. Fossati, M. Berghuis, J.N. Pelletier, Multiple conformers in active site of human dihydrofolate reductase F31R/Q35E double mutant suggest structural basis for methotrexate resistance, J. Biol. Chem. 284 (2009) 20079–20089.
[35] N.L. Allinger, Conformational analysis. 130. MM2. A hydrocarbon force field utilizing V1 and V2 torsional terms, J. Am. Chem. Soc. 99 (1977) 8127–8134.
[36] P. Labute, C. Williams, M. Feher, E. Sourial, J.M. Schmidt, Flexible alignment of small molecules, J. Med. Chem. 44 (2001) 1483–1490.